






RESEARCH ARTICLE | MARCH 15 2023

Characteristics of reattached oblique detonation induced by a double wedge

Kepeng Yao (姚克鹏) ; Pengfei Yang (杨鹏飞) ; Haoyang Li (李昊洋) ; Chun Wang (王春)  ; Zonglin Jiang (姜宗林) 



Physics of Fluids 35, 036112 (2023)

<https://doi.org/10.1063/5.0140177>



View
Online



Export
Citation



Biomicrofluidics
Special Topic:
Microfluidic Biosensors

Submit Today

Characteristics of reattached oblique detonation induced by a double wedge

Cite as: Phys. Fluids **35**, 036112 (2023); doi: 10.1063/5.0140177

Submitted: 27 December 2022 · Accepted: 22 February 2023 ·

Published Online: 15 March 2023



View Online



Export Citation



CrossMark

Kepeng Yao (姚克鹏),^{1,2} Pengfei Yang (杨鹏飞),³ Haoyang Li (李昊洋),^{1,2} Chun Wang (王春),^{1,2,a)} and Zonglin Jiang (姜宗林)^{1,2}

AFFILIATIONS

¹State Key Laboratory of High Temperature Gas Dynamics, Institute of Mechanics, Chinese Academy of Sciences, Beijing 100190, China

²School of Engineering Sciences, University of Chinese Academy of Sciences, Beijing 100049, China

³College of Engineering, Peking University, Beijing 100871, China

^{a)}Author to whom correspondence should be addressed: wangchun@imech.ac.cn

ABSTRACT

The stationary characteristics of the oblique detonation wave (ODW) induced by the double wedge with an expansion corner are investigated using two-dimensional Navier–Stokes equations along with a two-step induction-exothermic kinetic model. The results show that the detached ODW can be reattached by expansion waves induced by the double wedge so that the standing window of ODW can be expanded. The re-standing position of ODW depends on the location and strength of the expansion waves, which are governed by the first wedge length L and the corner angle between the first and second wedge surface θ_C . There is a critical angle reattachment that determines whether the ODW can be reattached by expansion waves, and this critical angle increases as wedge length increases. However, the detached ODW cannot be reattached when the wedge length is increased to a critical value regardless of the wedge corner. The re-standing position moves downstream with the increment of θ_C until the last Mach wave tangent to the subsonic zone behind the strong overdriven ODW because no more Mach waves interact with the initiation zone. Moreover, the comparison of viscous and inviscid fields demonstrates that a shorter wedge length is necessary for the viscous field to reattach the ODW because the recirculation zone forms a gas wedge that extends the first wedge surface.

Published under an exclusive license by AIP Publishing. <https://doi.org/10.1063/5.0140177>

I. INTRODUCTION

Detonation is an extreme combustion wave that propagates at supersonic speed in combustible gas. Detonation has the advantages of rapid heat release and high thermal efficiency,¹ making it an ideal combustion mode for hypersonic air-breathing engines. The propulsion system based on detonation has a short combustion chamber and light weight. At present, three detonation engines have been proposed and widely studied. These are the pulse detonation engine (PDE),^{2,3} rotating detonation engine (RDE),^{4–6} and oblique detonation engine (ODE).^{7–11} In an ODE, an oblique detonation wave (ODW) induced by a wedge or cone is applied to release fuel energy.^{12,13} The ODE is self-ignited by the shock wave, has a simple structure, and is suitable for high-Mach flight.^{14,15}

Recent ODW research has mainly concentrated on the initiation structures^{16–25} and wavefronts instability^{26–32} of detonation induced by a semi-infinite wedge. Two initiation patterns^{33,34} are determined by the inflow Mach number (Ma) and wedge angle. One is the

smooth-transition pattern, in which the ODW and oblique shock wave (OSW) are connected by a curved shock wave; the other is the abrupt-transition pattern, in which the OSW is transformed into an ODW through a triple-wave point.²⁴ However, there are complex interactions in the ODE combustor caused by such factors as the shock waves, boundary layer, and detonation–expansion.^{9,10,22,35–38} An ODW with an abrupt initiation structure always has a shorter initiation length owing to the interaction between transverse shock waves and the boundary layer, while an ODW with a smooth initiation structure experiences less impact from the boundary layer.^{39,40}

The initiation structure of an ODW can transform from abrupt to smooth through expansion waves induced by a wedge corner.⁴¹ The initiation length decreases with increasing wedge length until it is longer than the initiation length of the ODW induced by a semi-infinite wedge.^{34,42} However, the decreased inflow Ma or wedge angle results in increased initiation length and transforms the initiation structure from smooth to abrupt.³⁵ The initiation structure becomes unstable

when the inflow Ma drops (or wedge angle rises) to a critical value, causing the ODW to travel upstream and fluctuate at the equilibrium point.⁴³ The unstable initiation structure can be re-stabilized by expansion waves induced by the wedge corner.^{44,45} The studies on the aforementioned phenomena have demonstrated that both wedge angle and inlet velocity determine the stationary nature of an ODW and that stable operation of an ODE requires the detonation waves to be initiated and confined in the combustor. However, there are still significant challenges with an ODE, such as the difficulty of achieving an attached ODW in a finite-length combustor at a lower flight velocity. The applied range of an ODE can be further extended when an attached ODW is initiated and confined in the combustor at a lower flight velocity. Therefore, it is necessary to investigate methods for controlling the detached ODW.

This work simulated an ODW induced by a double wedge with an expansion corner using two-dimensional Navier–Stokes equations together with a two-step chemical reaction model and analyzed the effects of the location and strength of expansion waves on the standing window of ODW. Unlike previous studies,^{34,41,42,44,46} this work uses a wedge angle greater than the ODW detachment angle, implying that a semi-infinite single wedge induces a detached ODW. The double wedge adopted in the current work was a simplified model of a combustor and nozzle of ODE such that this study can investigate the effects of the complex wave–system interactions in the ODE combustor, such as the interaction of shock-boundary, detonation–expansion, on the standing window⁴⁷ of ODW.

II. PHYSICAL MODEL AND MATHEMATICAL METHODS

Figure 1 shows the schematic of an ODE and its classic flow field in a combustor. The air is compressed by the OSW induced by the inlet wedge and is mixed with the fuel. The supersonic inflow mixture is compressed by the OSW induced by the combustor wedge, and the temperature and pressure increase further. The high temperature triggers the chemical reaction, which eventually results in an ODW. A transverse shock wave (T-shock) is generated and connected with the OSW-to-ODW transition point for abrupt initiation. This paper focuses on the ODW structure and its stability in the combustor, assuming a homogeneous combustible mixture as the inflow.

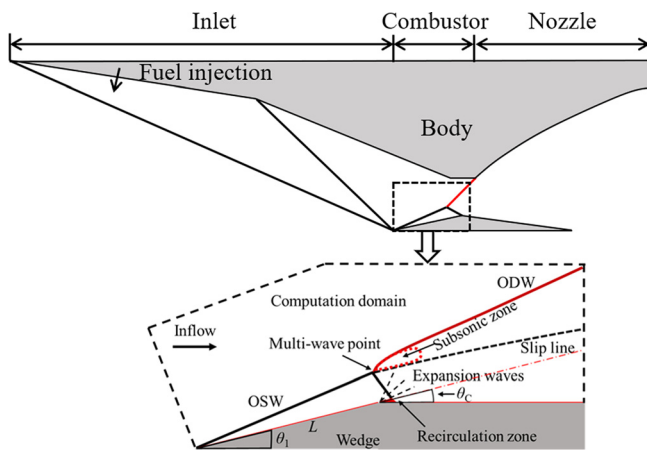


FIG. 1. Schematic of an ODE and its classic flow field in the combustor.

The simulation is based on the Navier–Stokes equations together with a two-step chemical kinetic model to simplify chain-branching kinetics.⁴⁸ This kinetic model belongs to an overall reaction mechanism. It is used in two ways: One is to simplify detailed reaction mechanisms and improve computational efficiency for complex phenomena; another goal is to investigate the complex wave–system interaction of initiation zone, in which the structures can be controlled through adjust some key chemical parameters. This study focuses on the interaction of expansion waves and subsonic zone behind the strong overdriven ODW. The results and conclusions could be more general to some extent. This two-step reaction model introduces two variables, ξ and λ , to describe the induction reaction and exothermic reaction, respectively. The two corresponding reaction rates, ω_ξ and ω_λ , are computed using the Arrhenius formula for chemical reactions. The governing two-dimensional Navier–Stokes equations and chemical reaction model are

$$\frac{\partial \rho}{\partial t} + \frac{\partial \rho u_j}{\partial x_j} = 0, \tag{1}$$

$$\frac{\partial \rho u_i}{\partial t} + \frac{\partial \rho u_i u_j}{\partial x_j} + p \delta_{ij} = \frac{\partial \tau_{ij}}{\partial x_j}, \tag{2}$$

$$\frac{\partial \rho e}{\partial t} + \frac{\partial \rho u_j e}{\partial x_j} + p u_j = \frac{\partial u_j \tau_{ij}}{\partial x_j} + \frac{\partial k \partial T}{\partial x_j x_j}, \tag{3}$$

$$\frac{\partial \rho \xi}{\partial t} + \frac{\partial \rho \xi u_j}{\partial x_j} = \omega_\xi, \tag{4}$$

$$\frac{\partial \rho \lambda}{\partial t} + \frac{\partial \rho \lambda u_j}{\partial x_j} = \omega_\lambda \tag{5}$$

with

$$\tau_{ij} = \mu \left(\left(\frac{\partial u_i}{\partial x_j} + \frac{\partial u_j}{\partial x_i} \right) - \frac{2}{3} \frac{\partial u_k}{\partial x_k} \delta_{ij} \right), \tag{6}$$

$$\omega_\xi = H(1 - \xi) \rho k_I \exp \left[\frac{E_I}{R} \left(\frac{1}{T_s} - \frac{1}{T} \right) \right], \tag{7}$$

$$\omega_\lambda = [1 - H(1 - \xi)] \rho (1 - \lambda) k_R \exp \left(\frac{-E_R}{RT} \right), \tag{8}$$

where E_I and E_R are the activation energies of the induction and exothermic reactions, respectively. The induced region is made to have dimensionless unit length by adjusting the value of the induced reaction rate constant $k_I = -U_{VN}$, where U_{VN} is the post-shock particle velocity in the shock fixed frame for the corresponding Chapman–Jouguet (C–J) detonation. The value of U_{VN} is calculated by the following equations:

$$U_{VN} = \sqrt{\gamma} \times \frac{2 + (\gamma - 1)M_{CJ}^2}{(\gamma + 1)M_{CJ}}, \tag{9}$$

$$M_{CJ}^2 = \left(1 + \frac{\gamma^2 - 1}{\gamma} Q \right) + \left[\left(1 + \frac{\gamma^2 - 1}{\gamma} Q \right)^2 - 1 \right]^{\frac{1}{2}}. \tag{10}$$

The exothermic reaction rate constant is selected as $k_R = 3.0$, which is used to control the length of the exothermic reaction zone, and H is the Heaviside step function

$$H(1 - \xi) = \begin{cases} 1, & \xi < 1, \\ 0, & \xi \geq 1. \end{cases} \quad (11)$$

The gas equation of state and the energy definition are

$$p = \rho RT, \quad (12)$$

$$e = \frac{RT}{\gamma - 1} + \frac{u_j u_j}{2} + (1 - \lambda)Q, \quad (13)$$

where δ_{ij} is the Kronecker delta and the variables ρ , u_j , e , T , p , γ , R , and Q are the density, velocity in the j -direction, specific total energy, temperature, pressure, specific heat ratio, gas constant, and total chemical energy available in the mixture, respectively. All the variables are non-dimensionalized by reference to the unburnt state of the gas mixture

$$\rho = \frac{\bar{p}}{\rho_0}, \quad p = \frac{\bar{p}}{p_0}, \quad T = \frac{\bar{T}}{T_0}, \quad u_j = \frac{\bar{u}_j}{\sqrt{R_0 T_0}}, \quad R = \frac{\bar{R}}{R_0}. \quad (14)$$

The main chemical parameters are set as

$$Q = 25, \quad E_I = 6.0T_s, \quad E_R = 1.0T_s, \quad \gamma = 1.3, \quad R_0 = 397, \quad (15)$$

where T_s is the temperature jump across the leading shock of Chapman–Jouguet (C–J) detonation wave; the variables E_I , E_R , and Q are non-dimensionalized by $R_0 T_0$; and the viscosity μ is computed via the Sutherland equation.¹¹ The chemical parameters are modeled by a detailed reaction kinetics of the hydrogen/air mixture. The wedge surface is modeled as a no-slip wall boundary for viscous field simulation. The left and upper boundaries are modeled as inlet boundaries with specific parameters, while the right boundary is a supersonic outlet boundary. The laminar flow model is adopted to simulate the viscous field in this paper. Although the boundary layer will undoubtedly become turbulent over a long downstream distance, a qualitative study assuming laminar flow should be sufficient to simulate the main wave structure of the ODW field over a short range in the flow direction.⁴⁰

In this work, the governing equations are numerically solved using the dispersion-controlled dissipation (DCD) scheme⁴⁹ with a second-order Runge–Kutta algorithm, and the convection terms are treated with Steger–Warming flux splitting.⁵⁰ The DCD scheme is a total variation-diminishing scheme that achieves second-order accuracy in a smooth field when the numerical dispersion is adjusted near the shock wave, which is used to simulate the detonation field widely.^{17,18,30,32,51} The grid width of the outer boundary layer is $\Delta = 0.1$, and the grid width of the first boundary layer is $\Delta_1 = 0.01$. The growth rate of the grid width is 1.01. The time step is satisfied to the Courant–Friedrichs–Lewy (CFL) condition to make the solving process converge stably, which is determined by the CFL condition. The CFL number is fixed at 0.3.

III. RESULTS AND DISCUSSION

A. Basic structures and grid resolutions

The baseline case $M_0 = 8$ was simulated with the Euler equations; the temperature contours are presented in Fig. 2. In this simulation, the inflow direction was at an angle of 30° from the x -axis. The multi-wave point at which the OSW-to-ODW transition occurred was at approximately $x = 35$. The T-shock was reflected as it interacted with the wedge surface. The reflected shock wave interacted with the slip line, forming a transmission shock that interacted with the ODW,

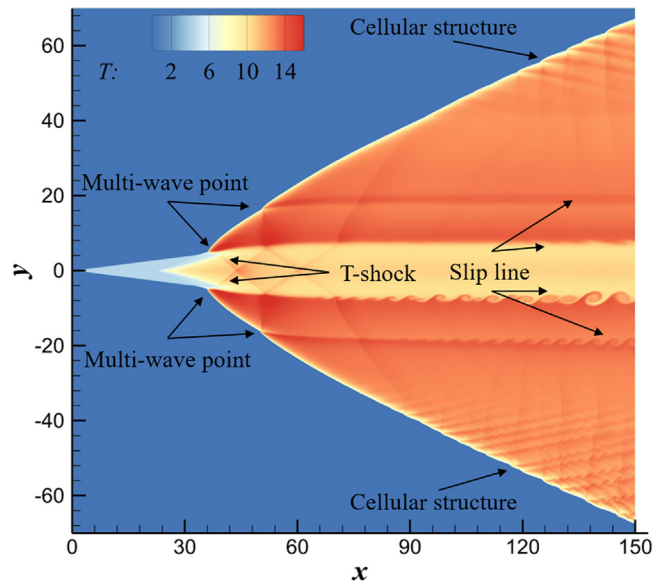


FIG. 2. Temperature contours generated with different grids for $M_0 = 8$. The grid scales are 0.1 (upper) and 0.05 (lower).

resulting in the formation of a new multi-wave point. Because of the downstream wavefront instability, more T-shocks were generated, resulting in a “saw-tooth” structure on the wave surface.^{29,30}

The grid independence of numerical simulation was tested and validated. The numerical cases were simulated using two grid resolutions with dimensionless grid scales of 0.1 and 0.05, corresponding to 10 and 20 grids in the induction zone of C–J detonation. The temperature contours are shown in Fig. 2. The multi-wave points, T-shock, and reflected shock wave with different resolutions almost exactly coincide. However, for a grid-scale of 0.05, the cellular structure at the wavefront is early, and vortexes are observed in the slip line owing to the Kelvin–Helmholtz (K–H) instability.

To quantify the effect of grid resolution, the pressure and temperature distributions were extracted along the wedge and the lines $y = 10$ and 20 in the flow field; these distributions are presented in Fig. 3. The pressure and temperature distributions for the grid scale of 0.1 are shown here as solid and dashed red curves, respectively. The black curves are the corresponding distributions for a grid-scale of 0.05. According to Fig. 3(a), the ODW fronts between $y = 10$ and 20 approximately coincide for both grid resolutions. According to Fig. 3(b), the pressure and temperature distributions along the wedge coincide for both resolutions. Although the structure was more refined with a grid scale of 0.05, the ODW standing state is unaffected by this small-scale refinement. Therefore, a maximum grid scale of 0.1 was used to strike a balance between simulation accuracy and processing efficiency. On the basis of the above, the grid resolution used in this investigation is appropriate.

For the single-wedge geometry, the wedge angle and inflow Mach number M_0 are crucial to the initiation structure and the stability of the ODW. For the oblique detonation induced by the single semi-infinite wedge, there are two critical angles, C–J wedge-angle θ_{CJ} and detached angle θ_d , when the inflow Mach number is constant. The attached ODW will be induced by the wedge when the wedge

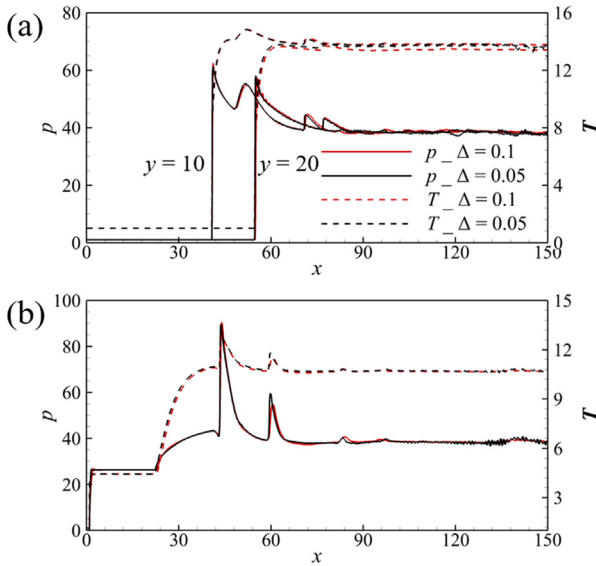


FIG. 3. Pressure and temperature distributions in the flow field (a) along the lines $y = 10$ and 20 and (b) along the wedge.

angle is between θ_{C1} and θ_{d1} , which is the standing window of ODW. A detached ODW can be observed if the wedge angle is greater than a critical detachment angle θ_d for a specific M_0 , and a strong overdriven ODW at the initiation zone is observed. The critical detachment angle can be obtained by the detonation polar curve, which is computed by Eq. (16). According to the detonation polar curves in Fig. 4, the ODW detachment angle is 34.2° for $M_0 = 8$ and 28.9° for $M_0 = 7$. The wedge angle in this study is fixed at 30° , which is greater than the detachment angle for $M_0 = 8$ and smaller than that for $M_0 = 7$. As a result, the ODW is detached when $M_0 = 7$. Figure 5 is the diagram of the detached ODW field induced by the single wedge. The OSW has transitioned to an ODW through a multi-wave point, a case similar to the attached ODW with its abrupt transition structure. In contrast to the attached scenario, the ODW continuously travels upstream

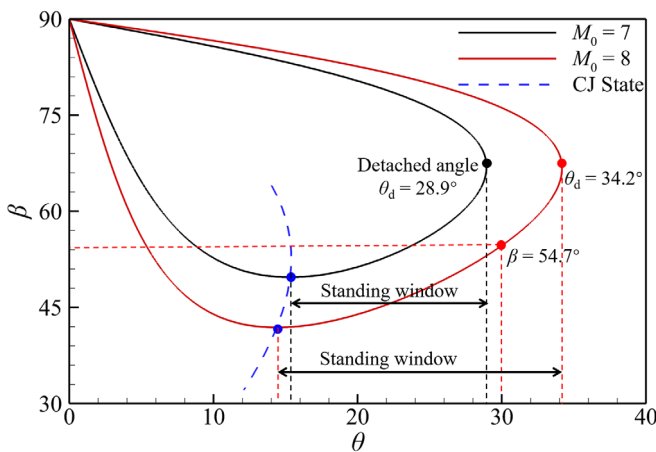


FIG. 4. Detonation polar curves for $M_0 = 7$ and 8 .

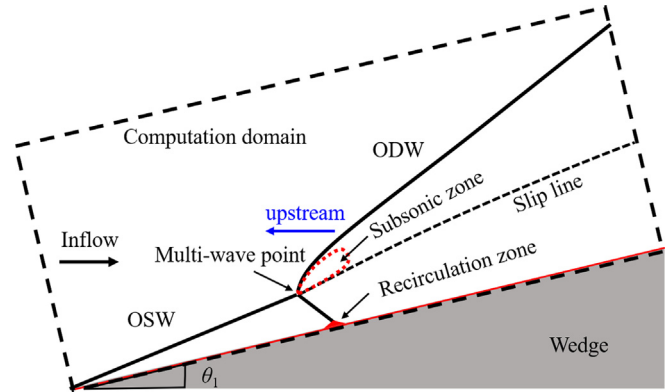


FIG. 5. Diagram of the detached ODW field induced by the single wedge.

because the wedge angle is greater than the detached angle, causing the ODW to enter a state of thermal choking. Furthermore, the recirculation zone caused by the interaction of the T-shock with the boundary layer worsens the ODW instability

$$\frac{\tan \beta}{\tan \beta - \theta} = \frac{(\gamma + 1)M_0^2 \sin^2 \beta}{\gamma M_0^2 \sin^2 \beta + 1 \pm \sqrt{(M_0^2 \sin^2 \beta - 1)^2 - 2Q \left(\gamma - \frac{1}{\gamma}\right) M_0^2 \sin^2 \beta}} \quad (16)$$

B. Reattached ODW induced by the double wedge

The detached ODW may be reattached when the expansion waves induced by the wedge corner interact with the strong overdriven ODW in the initiation zone. Figure 6 depicts the effect of the first wedge length and wedge corner on the ODW standing state induced by the double wedge. When the wedge length is $L = 66$ and the corner is $\theta_C = 30^\circ$, the induced ODW stands on the wedge, whereas the ODW induced by the single wedge with wedge angle $\theta_1 = 30^\circ$ is detached from the detonation polar curve, as shown in Fig. 6(a). As illustrated in Figs. 6(b) and 6(c), the ODW remains detached when the wedge length is increased to $L = 70$ or the corner is decreased to $\theta_C = 25^\circ$. The temperature contours of the ODW field with $L = 70$ and $\theta_C = 40^\circ$ are shown in Fig. 6(d). The ODW in this figure is reattached by the double wedge, and the recirculation zone is smaller than in Fig. 6(a). From the preceding four cases, it is reasonable to infer that both the wedge length L and corner θ_C determine whether the ODW can be reattached by the expansion waves.

Figure 7 illustrates the effect of the wedge length and second wedge angle on the initiation length of the reattached ODW induced by a double wedge. Figure 7(a) shows the temperature contours of the ODW field induced by a double wedge with $L = 64$ and $\theta_C = 25^\circ$ (black curve) and 30° (red curve), and $L = 66$ and $\theta_C = 30^\circ$ (blue curve). The initiation structures of these cases are similar, but the initiation lengths are different. The initiation length is longest for $L = 64$ and $\theta_C = 30^\circ$ and shortest for $L = 66$ and $\theta_C = 30^\circ$. We can conclude that the initiation length increases with decreasing wedge length and

08 April 2024 03:22:30

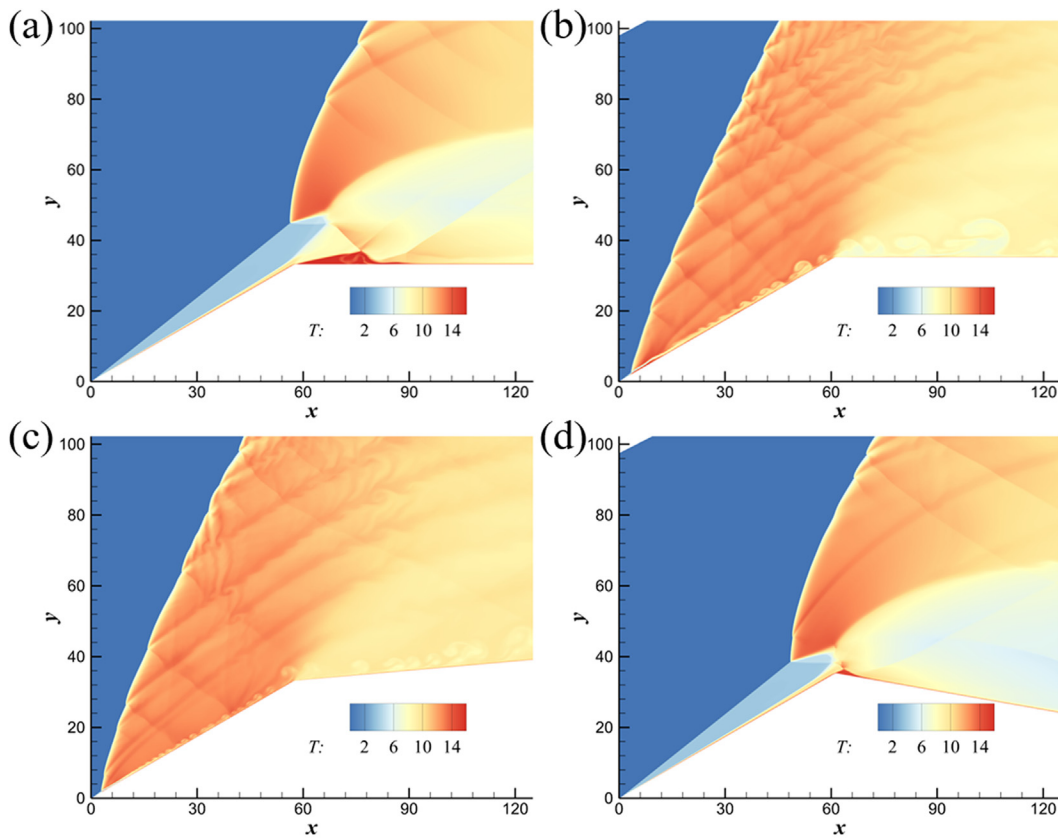


FIG. 6. Temperature contours of the ODW field induced by the double wedge with (a) $L = 66$ and $\theta_C = 30^\circ$, (b) $L = 70$ and $\theta_C = 30^\circ$, (c) $L = 66$ and $\theta_C = 25^\circ$, and (d) $L = 70$ and $\theta_C = 40^\circ$.

increasing corner. Figure 7(b) shows the temperature contours of the ODW fields induced by double wedges with $L = 70$ and $\theta_C = 50^\circ$ (black curve), $L = 70$ and $\theta_C = 40^\circ$ (red curve), and $L = 68$ and $\theta_C = 40^\circ$ (blue curve). The initiation lengths with $L = 70$ and $\theta_C = 50^\circ$ and 40° are coincident and shorter than with $L = 68$ and $\theta_C = 40^\circ$.

To make a quantitative comparison, we extracted the pressure distributions along the wedge and the line $y = 60$, as shown in Fig. 8. The expansion waves induced by the wedge corner cause a sharp drop in pressure along the wedge surface. The amplitude and position of the pressure drop are determined by the interaction area and location of the expansion waves, respectively. The pressure distribution along the wedge is coincident before the corner for different θ_C values, while the pressure more sharply drops after the corner for $L = 64$ and $\theta_C = 30^\circ$ than for $L = 64$ and $\theta_C = 25^\circ$. This means that the expansion fan region is larger for $\theta_C = 30^\circ$ and $L = 64$. According to the pressure distribution along the line $y = 60$ in Fig. 8(a), the ODW initiation position is determined by the wedge length and corner, which, respectively, regulate the location and interaction region of expansion waves. However, the initiation length does not increase when the wedge corner is increased from $\theta_C = 40^\circ$ to $\theta_C = 50^\circ$ for the cases with $L = 70$, although the expansion fan region is different, as shown in Fig. 8(b). For the cases with $\theta_C = 40^\circ$, the initiation position moves downstream when the wedge length is decreased from $L = 70$ to $L = 68$. We can

deduce from this that the ODW can be reattached using a double wedge, and reattachment is determined by the wedge length and corner. The initiation length increases with decreasing wedge length. However, the effect of the wedge corner θ_C on the initiation length is uncertain.

C. Discussion on the ODW reattachment mechanism

The transverse shock wave interacts with the boundary layer and generates a recirculation zone, which can be regarded as a gas wedge called an “equivalent wedge” in this paper. The recirculation zone plays an important role in ODW instability. The wave structures of an ODW induced by a double wedge with $L = 70$ are displayed in Fig. 9. For $\theta_C = 30^\circ$, the ODW is initiated and moves upstream [as shown in Fig. 6(b)], so the detached ODW cannot be reattached by expansion waves in this scenario. An attached ODW is observed when θ_C is increased to 50° , as shown in Fig. 9(b). Figure 9(a) shows the critical position of the ODW ($t = 106.2$). The recirculation zone is observed to be equivalent to a gas wedge, and the angle is approximately identical to the wedge angle. This indicates that the recirculation zone extends the first wedge length. For $\theta_C = 50^\circ$, the wedge combines with the recirculation zone and forms a pseudo-double-wedge. The detached ODW is also reattached, as depicted in Fig. 9(b). Therefore, a shorter

08 April 2024 03:22:30

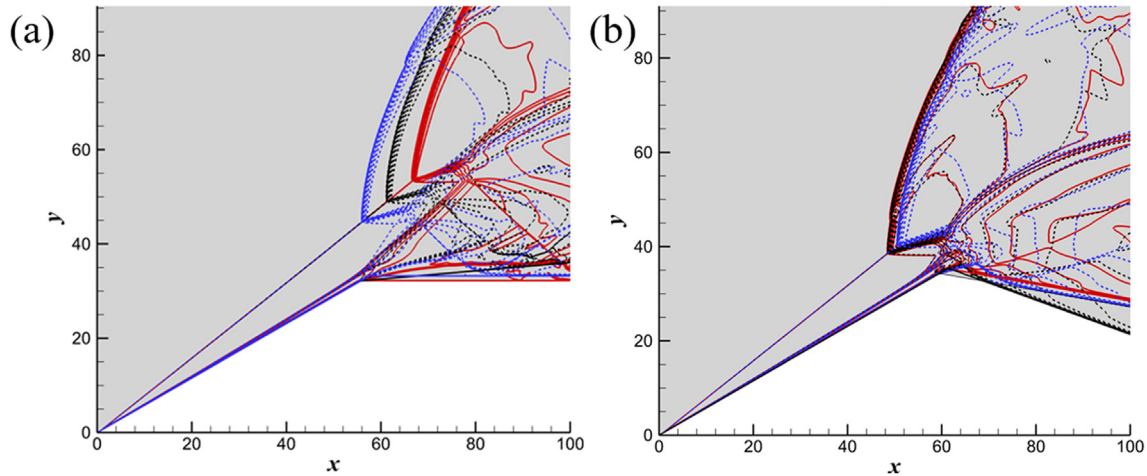


FIG. 7. Temperature contours of the reattached ODW induced by a double wedge with (a) $L = 64$ and $\theta_c = 25^\circ$ (black curve) and 30° (red curve), and $L = 66$ and $\theta_c = 30^\circ$ (blue curve); (b) $L = 70$ and $\theta_c = 50^\circ$ (black curve) and 40° (red curve), and $L = 68$ and $\theta_c = 40^\circ$ (blue curve).

wedge is necessary to reattach the ODW in a viscous field owing to the recirculation zone generated by the interaction between the T-shock and the boundary layer, which is also illustrated in Appendix B.

The red dashed curves in Fig. 10 represent the sonic lines, while the areas enclosed by the red curves are subsonic zones. The Mach lines represent the upper critical position of the region influenced by the disturbances in the supersonic field and are indicated by the blue curves.

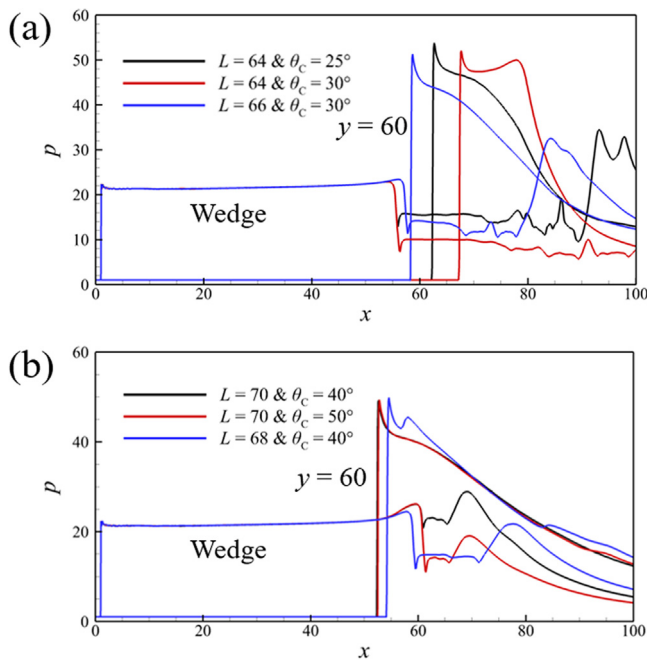


FIG. 8. Field pressure distributions along the line $y = 60$ and the wedge surface for (a) $L = 64$ and $\theta_c = 25^\circ$ (black curve) and 30° (red curve), and $L = 66$ and $\theta_c = 30^\circ$ (blue curve); (b) $L = 70$ and $\theta_c = 50^\circ$ (black curve) and 40° (red curve), and $L = 68$ and $\theta_c = 40^\circ$ (blue curve).

This figure shows that the disturbances affect the initiation zone when the Mach lines intersect the subsonic zone. In this work, the disturbances are mainly induced by the wedge corner and act on the leading shock wave via expansion waves. Notably, Mach lines only exist in the supersonic flow field because the disturbance affects all the fields in the subsonic flow region (as explained in Appendix A). Therefore, the expansion wave must interact with the initiation zone of ODW if change the standing state and position of the detonation wave. The corresponding recirculation zone is generated by the interaction of the T-shock with the viscous boundary layer. The equivalent wedge corner formed by this recirculation zone is less than the actual corner. The expansion waves induced by the wedge corner can directly interact with the strong overdriven section of ODW and reduce its strength when the first wedge length is shorter (e.g., less than the oblique detonation induction length). However, it maybe changes the initiation structure and even quenches the ODW.⁴¹ With the increase in the first wedge length, the position of the expansion waves gradually moves downstream so that the expansion waves cannot directly interact with the strong overdriven ODW. However, it can reduce the strength of the strong overdriven ODW when expansion waves interact with the subsonic zone behind the strong overdriven ODW, as shown in Fig. 10. The initiation structures of the detonation field induced by the double wedge with $L = 64$ are depicted in Figs. 10(a) and 10(b) for $\theta_c = 25^\circ$ and $\theta_c = 30^\circ$, respectively. As illustrated in Fig. 10(a), all the Mach lines originating from the wedge corner interact with the subsonic zone behind the ODW. The initiation length is shorter owing to a wider region of Mach waves interacting with the subsonic zone when the wedge corner is increased to $\theta_c = 30^\circ$, as shown in Fig. 10(b). According to Figs. 10(c) and 10(d), some Mach lines originate from the wedge corner that does not interact with the subsonic zone. This further increases the wedge corner but does not increase the initiation length of the reattached ODW. The behavior is similar in Fig. 10(b), where the initiation location remains unchanged when the second wedge angle is further increased to $\theta_c = 40^\circ$. (The diagram is not shown in this paper.)

The corner angle dominates the expansion fan according to gas dynamics, and the last Mach wave deflects clockwise as θ_c increases.

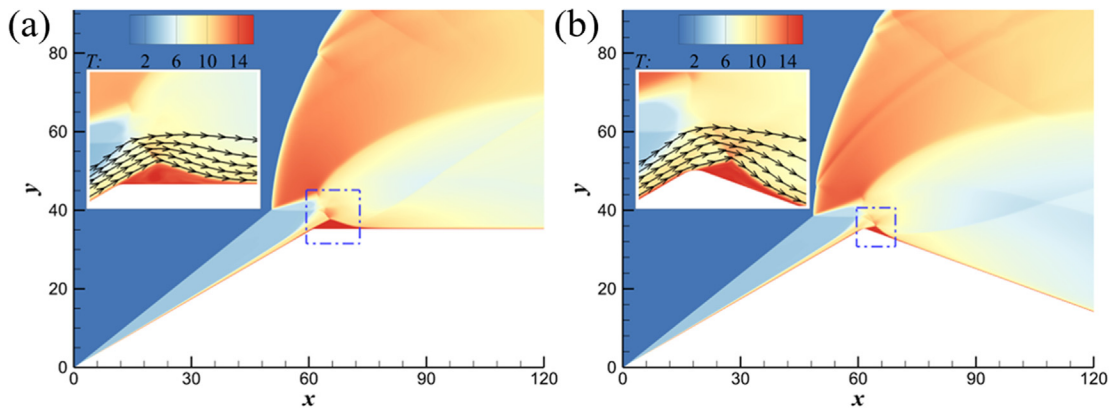


FIG. 9. Temperature contours of an ODW field induced by a double wedge with $L = 70$ and (a) $\theta_C = 30^\circ$ (detached) and (b) $\theta_C = 50^\circ$ (reattached).

The expansion waves affect the initiation zone only when it interacts with the subsonic zone behind overdriven detonation. The ODW moves upstream owing to thermal choking if the wedge angle is greater than the detachment angle. The thermal choking behind the ODW may be weakened (or eliminated) by the expansion waves. Additionally, the interaction area of expansion waves and the subsonic zone causes a shorter initiation length, as indicated in Figs. 11(a) and 11(b). The initiation length is unaffected

by the wedge corner when it is increased to a critical value, as shown in Fig. 11(b), where the last Mach wave is tangent to the subsonic zone behind the overdriven detonation. Further increasing θ_C does not cause the initiation position to move downstream because no more Mach waves are interacting with the initiation zone, as illustrated in Figs. 11(b) and 11(c). We can conclude that there are two critical values—one that determines whether the ODW can be reattached by expansion waves and another one determines whether the ODW initiation length can be altered by the wedge corner θ_C .

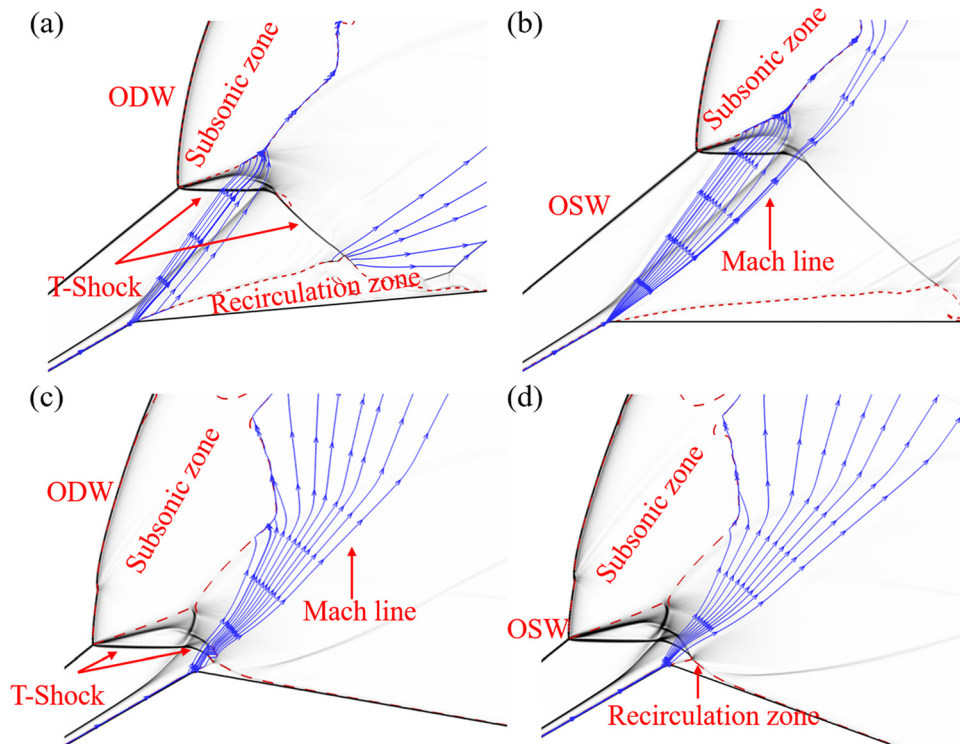


FIG. 10. Initiation structure of the detonation field for (a) $L = 64$ and $\theta_C = 25^\circ$, (b) $L = 64$, and $\theta_C = 30^\circ$, (c) $L = 70$ and $\theta_C = 40^\circ$, and (d) $L = 70$ and $\theta_C = 50^\circ$. The red curves are sonic lines, and the blue curves are Mach lines.

08 April 2024 03:22:30

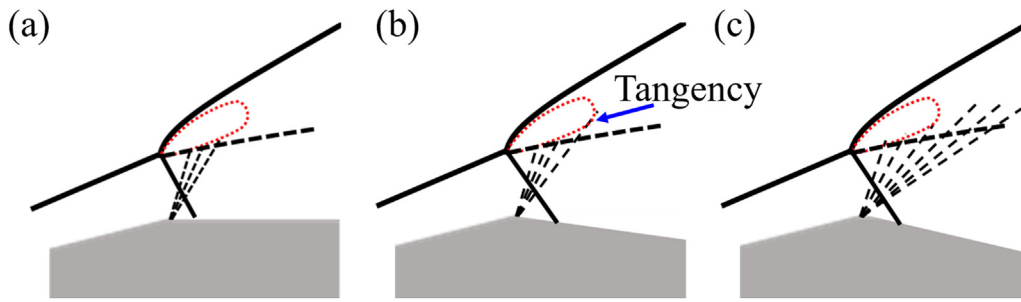


FIG. 11. Three situations in which expansion waves interact with the subsonic zone. The relationship between the last Mach wave and subsonic zone: (a) intersectant, (b) tangent, and (c) non-intersectant.

The critical reattachment angle θ_C determines whether the ODW can be reattached. Figure 12 shows θ_C as a function of the wedge length L . Whereas the black curve indicates that ODWs can be reattached by expansion waves, the red curve indicates that ODWs cannot be reattached by expansion waves. Between these two curves, there is a critical reattachment curve. This demonstrates that the critical reattachment angle increases as the wedge length increases. It should be noted that the detached ODW cannot be reattached when $L \geq 72$ even if the wedge corner is very large. The expansion waves do not interact with the initiation zone so that cannot reduce the strength of strong overdriven ODW. The expansion disturbance can only decrease the angle of the downstream ODW but cannot change the stationary state and position of the detonation wave.

IV. CONCLUSION

According to the detonation polar line, the attached oblique detonation wave will be observed when the inflow Mach number is larger than the critical Mach number, while the detached oblique detonation wave will be induced when the inflow Mach number is less than that. This work simulated the ODW induced by the double wedge with an expansion corner by solving the Navier–Stokes equations together with a two-step induction-exothermic chemical reaction kinetic mode. The findings demonstrate that the wedge corner-induced expansion waves can reattach a detached ODW and that the initiation length is sensitive to the position and interaction region of these waves. The ODW initiation length increases with decreasing wedge length. The

initiation length does not increase as the wedge corner increases because no more Mach waves interact with the subsonic zone when the last Mach wave is tangent to the subsonic zone. A shorter wedge is required to reattach the detached ODW owing to the recirculation zone generated by the interaction between the T-shock and boundary layer extending to the first wedge surface. In addition, the critical reattachment angle increases with increasing wedge length. When the wedge corner is larger than the critical reattachment angle, the detached ODW can be reattached by the expansion waves. The interaction region between the expansion waves and the initiation zone is inadequate to reattach the detached ODW if the wedge is too long, even when the wedge corner is very large. This work demonstrates that the standing window of the ODW may be expanded using a double wedge to induce it, which reduces the lowest critical Mach number of an ODE. However, there are complicated interactions of wave and system, which include the expansion waves, strong overdriven oblique detonation wave, compress waves, and combustion waves, such that is hard to deduce the quantitative formula of stability of ODW. Further works should be carried out based on this work, and more numerical simulations and theoretical analysis are required to establish a quantitative theory formula to control the stability of ODW.

ACKNOWLEDGMENTS

This work was supported by the National Natural Science Foundation of China (Grant Nos. 12072353, 12132017, and 12202014).

AUTHOR DECLARATIONS

Conflict of Interest

The authors have no conflicts to disclose.

Author Contributions

Kepeng Yao: Formal analysis (equal); Investigation (equal); Software (equal); Validation (equal); Writing – original draft (equal). **Pengfei Yang:** Formal analysis (equal); Investigation (equal); Methodology (equal); Writing – original draft (supporting). **Haoyang Li:** Investigation (equal); Resources (equal); Validation (equal). **Chun Wang:** Formal analysis (equal); Methodology (equal); Resources (equal); Software (equal); Writing – original draft (equal). **Zonglin Jiang:** Project administration (equal); Software (supporting).

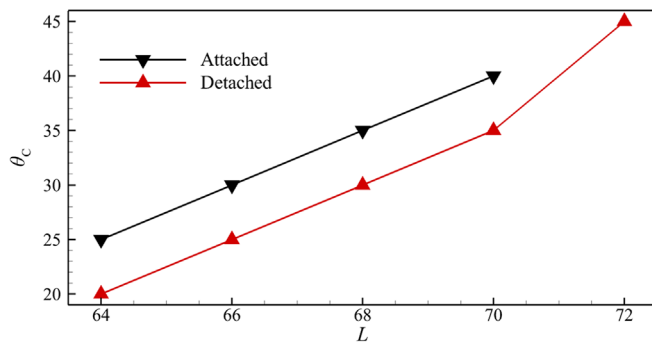


FIG. 12. Critical reattachment angle θ_C as a function of wedge length L .

08 April 2024 03:22:30

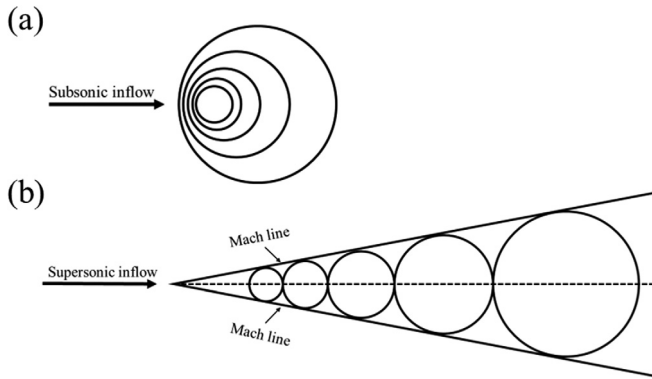


FIG. 13. Diagram of the disturbance propagates in (a) subsonic and (b) supersonic flow fields.

DATA AVAILABILITY

The data that support the findings of this study are available from the corresponding author upon reasonable request.

APPENDIX A: ANALYSIS OF MACH WAVES

The disturbance spreads at sonic speed in the field. The disturbance affects all the fields in the subsonic flow, and the region it affects is conical in the supersonic field, as illustrated in Fig. 13. However, the Mach core degenerates into two lines in the two-dimensional scenario, the two lines are Mach lines, which are used to analyze the effect of expansion waves on the ODW initiation length and reattachment. The upper Mach line angle α is calculated using the characteristic equation

$$\alpha = \arcsin\left(\frac{1}{M_{local}}\right) + \arctan\left(\frac{v}{u}\right), \quad (A1)$$

where M_{local} is the local Mach number. The Mach lines only appear in the supersonic flow field because the Mach core only exists there. As the numerical simulation is to solve the equations by discrete method, the flow field is discretized into grid points. The Mach line analysis method is very suitable to analyze the flow field affected by expansion disturbance. According to the definition of the Mach line and propagation characteristic of disturbance, the disturbances can spread to all subsonic regions if the Mach line crosses the subsonic zone.

APPENDIX B: SIMULATION RESULTS FOR AN INVISCID FIELD

The Euler equations, which are similar to the Navier–Stokes equations with zero viscosity μ , were solved to simulate inviscid flow fields. The wedge surface was modeled as a slip wall boundary for the inviscid field simulation. For inviscid cases with wedge length $L = 85$, the detached ODW cannot be reattached by the double wedge with $\theta_C = 25^\circ$, whereas an attached ODW is obtained for $\theta_C = 30^\circ$. Figure 14 shows the temperature contours of the reattached ODWs induced by a double wedge with $L = 85$ and θ_C

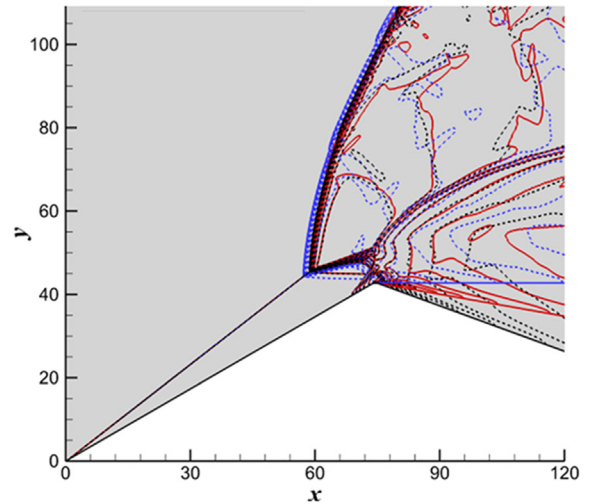


FIG. 14. Temperature contours of detonation induced by a double wedge with $L = 85$ and $\theta_C = 30^\circ$ (blue curve), 40° (red curve), and 50° (black curve) for an inviscid field.

$= 30^\circ, 40^\circ$, and 50° . Similar initiation structures can be observed. The initiation lengths coincide for $\theta_C = 40^\circ$ and 50° but are both longer than that for $\theta_C = 30^\circ$. This also matches the simulation results in Fig. 10.

Figure 15 shows the critical reattachment angle as a function of wedge length L for the inviscid field. The red curve represents ODWs that cannot be reattached by expansion waves, the black curve represents ODWs that can be reattached, and the critical reattachment curve is between these two curves. This demonstrates that the critical reattachment angle θ_C decreases with increasing wedge length L . Although θ_C is a relatively tiny value, the detached ODW cannot be reattached when the wedge length is increased to $L = 87$. The viscous field requires a shorter wedge than in the inviscid scenario, mostly owing to the presence of recirculation, which increases the whole wedge length and strengthens the ODW instability. Moreover, the streamwise induction length after the oblique shock wave is 72.9, which is smaller than the first wedge length of all inviscid cases to assure the initiation of ODW. However, the actual streamwise induction length in the viscous field is smaller

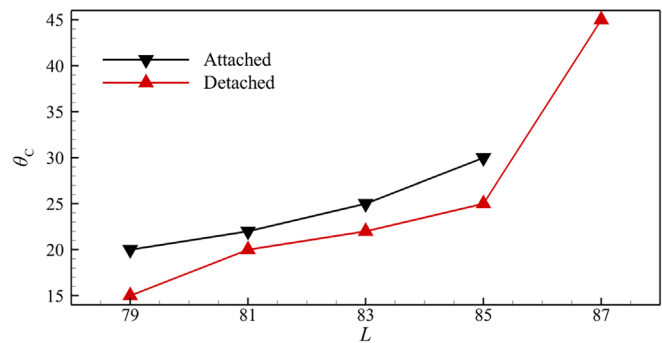


FIG. 15. Critical reattachment angle θ_C as a function of wedge length L for an inviscid field.

than this theory value because the boundary layer strengthens the oblique shock wave, and the temperature near the wedge surface is higher than the post-shock temperature of the inviscid field.

REFERENCES

- ¹P. Wolański, "Detonative propulsion," *Proc. Combust. Inst.* **34**, 125–158 (2013).
- ²F. Ma, J.-Y. Choi, and V. Yang, "Thrust chamber dynamics and propulsive performance of multitube pulse detonation engines," *J. Propul. Power* **21**, 681–691 (2005).
- ³J. Dai, F. Xu, X. Cai, and Y. Mahmoudi, "Effects of velocity shear layer on detonation propagation in a supersonic expanding combustor," *Phys. Fluids* **33**, 105110 (2021).
- ⁴M. Zhao, M. J. Cleary, and H. Zhang, "Combustion mode and wave multiplicity in rotating detonative combustion with separate reactant injection," *Combust. Flame* **225**, 291–304 (2021).
- ⁵R. Yokoo, K. Goto, J. Kim, A. Kawasaki, K. Matsuo, J. Kasahara, A. Matsuo, and I. Funaki, "Propulsion performance of cylindrical rotating detonation engine," *AIAA J.* **58**, 5107–5116 (2020).
- ⁶W. Zhu, Y. Wang, and J. Wang, "Flow field of a rotating detonation engine fueled by carbon," *Phys. Fluids* **34**, 073311 (2022).
- ⁷Z. Jiang, Z. Zhang, Y. Liu, C. Wang, and C. Luo, "The criteria for hypersonic airbreathing propulsion and its experimental verification," *Chin. J. Aeronaut.* **34**, 94–104 (2020).
- ⁸D. A. Rosato, M. Thornton, J. Sosa, C. Bachman, G. B. Goodwin, and K. A. Ahmed, "Stabilized detonation for hypersonic propulsion," *Proc. Natl. Acad. Sci. U.S.A.* **118**, e2102244118 (2021).
- ⁹Z. Zhang, Y. Liu, and C. Wen, "Mechanisms of the destabilized Mach reflection of inviscid oblique detonation waves before an expansion corner," *J. Fluid Mech.* **940**, A29 (2022).
- ¹⁰K. Wang, Z. Zhang, P. Yang, and H. Teng, "Numerical study on reflection of an oblique detonation wave on an outward turning wall," *Phys. Fluids* **32**, 046101 (2020).
- ¹¹L. Yang, L. Yue, D. Yu, and Z. Chen, "Numerical study on wave configuration of wedge-induced oblique detonation wave: Reactive boundary layer effect," *Phys. Fluids* **34**, 116103 (2022).
- ¹²P. Yang, H. D. Ng, H. Teng, and Z. Jiang, "Initiation structure of oblique detonation waves behind conical shocks," *Phys. Fluids* **29**, 086104 (2017).
- ¹³S. Miao, J. Zhou, Z. Lin, X. Cai, and S. Liu, "Numerical study on thermodynamic efficiency and stability of oblique detonation waves," *AIAA J.* **56**, 3112–3122 (2018).
- ¹⁴Z. Zhang, C. Wen, W. Zhang, Y. Liu, and Z. Jiang, "Formation of stabilized oblique detonation waves in a combustor," *Combust. Flame* **223**, 423–436 (2021).
- ¹⁵Z. Zhang, K. Ma, W. Zhang, X. Han, Y. Liu, and Z. Jiang, "Numerical investigation of a Mach 9 oblique detonation engine with fuel pre-injection," *Aerosp. Sci. Technol.* **105**, 106054 (2020).
- ¹⁶H. Teng, C. Tian, Y. Zhang, L. Zhou, and H. D. Ng, "Morphology of oblique detonation waves in a stoichiometric hydrogen-air mixture," *J. Fluid Mech.* **913**, A1 (2021).
- ¹⁷H. Teng, H. D. Ng, P. Yang, and K. Wang, "Near-field relaxation subsequent to the onset of oblique detonations with a two-step kinetic model," *Phys. Fluids* **33**, 096106 (2021).
- ¹⁸Y. Zhang, Y. Fang, H. D. Ng, and H. Teng, "Numerical investigation on the initiation of oblique detonation waves in stoichiometric acetylene-oxygen mixtures with high argon dilution," *Combust. Flame* **204**, 391–396 (2019).
- ¹⁹C. Li, K. Kailasanath, and E. S. Oran, "Detonation structures behind oblique shocks," *Phys. Fluids* **6**, 1600–1611 (1994).
- ²⁰Y. Fang, Y. Zhang, X. Deng, and H. Teng, "Structure of wedge-induced oblique detonation in acetylene-oxygen-argon mixtures," *Phys. Fluids* **31**, 026108 (2019).
- ²¹T. Wang, Y. Zhang, H. Teng, Z. Jiang, and H. D. Ng, "Numerical study of oblique detonation wave initiation in a stoichiometric hydrogen-air mixture," *Phys. Fluids* **27**, 096101 (2015).
- ²²Q. Qin and X. Zhang, "A novel method for trigger location control of the oblique detonation wave by a modified wedge," *Combust. Flame* **197**, 65–77 (2018).
- ²³Q. Qin and X. Zhang, "Study on the initiation characteristics of the oblique detonation wave by a co-flow hot jet," *Acta Astronaut.* **177**, 86–95 (2020).
- ²⁴Z. Luan, Y. Huang, R. Deiterding, and Y. You, "On the evolutions of triple point structure in wedge-stabilized oblique detonations," *Phys. Fluids* **34**, 067118 (2022).
- ²⁵J. Sun, P. Yang, B. Tian, and Z. Chen, "Effects of wedge-angle change on the evolution of oblique detonation wave structure," *Phys. Fluids* **34**, 096112 (2022).
- ²⁶J. Choi, D. Kim, I. Jeung, F. Ma, and V. Yang, "Cell-like structure of unstable oblique detonation wave from high-resolution numerical simulation," *Proc. Combust. Inst.* **31**, 2473–2480 (2007).
- ²⁷J. Verreault, A. J. Higgins, and R. A. Stowe, "Formation of transverse waves in oblique detonations," *Proc. Combust. Inst.* **34**, 1913–1920 (2013).
- ²⁸H. Teng, Z. Jiang, and H. D. Ng, "Numerical study on unstable surfaces of oblique detonations," *J. Fluid Mech.* **744**, 111–128 (2014).
- ²⁹Y. Zhang, L. Zhou, J. Gong, H. D. Ng, and H. Teng, "Effects of activation energy on the instability of oblique detonation surfaces with a one-step chemistry model," *Phys. Fluids* **30**, 106110 (2018).
- ³⁰P. Yang, H. D. Ng, and H. Teng, "Unsteady dynamics of wedge-induced oblique detonations under periodic inflows," *Phys. Fluids* **33**, 016107 (2021).
- ³¹W. Han, C. Wang, and C. K. Law, "Three-dimensional simulation of oblique detonation waves attached to cone," *Phys. Rev. Fluids* **4**, 053201 (2019).
- ³²P. Yang, H. Li, Z. Chen, C. Wang, and H. Teng, "Numerical investigation on movement of triple points on oblique detonation surfaces," *Phys. Fluids* **34**, 066113 (2022).
- ³³H. Teng and Z. Jiang, "On the transition pattern of the oblique detonation structure," *J. Fluid Mech.* **713**, 659–669 (2012).
- ³⁴M. V. Papalexandris, "A numerical study of wedge-induced detonations," *Combust. Flame* **120**, 526–538 (2000).
- ³⁵Y. Gao, H. Li, G. Xiang, and S. Peng, "Initiation characteristics of oblique detonation waves from a finite wedge under argon dilution," *Chin. J. Aeronaut.* **34**, 81–90 (2021).
- ³⁶S. Miao, D. Xu, T. Song, and J. Yu, "Shock wave-boundary layer interactions in wedge-induced oblique detonations," *Combust. Sci. Technol.* **192**, 2345–2370 (2019).
- ³⁷L. Yang, L. Yue, and Q. Zhang, "Onset of oblique detonation waves for a cavity-based wedge," *AIAA J.* **60**, 1–14 (2022).
- ³⁸Q. Qin and X. Zhang, "Controllable initiation characteristics of the oblique detonation wave in a combustor with a confined cone of a novel structure," *Aerosp. Sci. Technol.* **107**, 106267 (2020).
- ³⁹Y. Fang, Z. Zhang, and Z. Hu, "Effects of boundary layer on wedge-induced oblique detonation structures in hydrogen-air mixtures," *Int. J. Hydrogen Energy* **44**, 23429–23435 (2019).
- ⁴⁰G. Li, G. Zhang, Y. Zhang, L. Ji, and S. Gao, "Influence of viscous boundary layer on initiation zone structure of two-dimensional oblique detonation wave," *Aerosp. Sci. Technol.* **104**, 106019 (2020).
- ⁴¹G. Xiang, X. Gao, W. Tang, X. Jie, and X. Huang, "Numerical study on transition structures of oblique detonations with expansion wave from finite-length cowl," *Phys. Fluids* **32**, 056108 (2020).
- ⁴²G. Xiang, X. Li, X. Sun, and X. Chen, "Investigations on oblique detonations induced by a finite wedge in high altitude," *Aerosp. Sci. Technol.* **95**, 105451 (2019).
- ⁴³P. Yang, H. Teng, Z. Jiang, and H. D. Ng, "Effects of inflow Mach number on oblique detonation initiation with a two-step induction-reaction kinetic model," *Combust. Flame* **193**, 246–256 (2018).
- ⁴⁴K. Yao, C. Wang, and Z. Jiang, "A numerical study of oblique detonation re-stabilization by expansion waves," *Aerosp. Sci. Technol.* **122**, 107409 (2022).
- ⁴⁵J. Y. Choi, E. J. R. Shin, and I.-S. Jeung, "Unstable combustion induced by oblique shock waves at the non-attaching condition of the oblique detonation wave," *Proc. Combust. Inst.* **32**, 2387–2396 (2009).
- ⁴⁶Y. Fang, Z. Hu, and H. Teng, "Numerical investigation of oblique detonations induced by a finite wedge in a stoichiometric hydrogen-air mixture," *Fuel* **234**, 502–507 (2018).
- ⁴⁷Z. Xu, G. Dong, Z. Pan, and M. Gui, "Standing window of oblique detonation with pathological behaviour," *Chin. J. Aeronaut.* **34**, 496–503 (2021).

- ⁴⁸H. D. Ng, M. I. Radulescu, A. J. Higgins, N. Nikiforakis, and J. H. S. Lee, "Numerical investigation of the instability for one-dimensional Chapman–Jouguet detonations with chain-branching kinetics," *Combust. Theory Model.* **9**, 385–401 (2005).
- ⁴⁹Z. Jiang, "On dispersion-controlled principles for non-oscillatory shock-capturing schemes," *Acta Mech. Sin.* **20**, 1–15 (2004).
- ⁵⁰J. L. Steger and R. F. Warming, "Flux vector splitting of the inviscid gas-dynamic equations with application to finite-difference methods," *J. Comput. Phys.* **40**, 263–293 (1981).
- ⁵¹W. Zhang, Z. Zhang, Z. Jiang, X. Han, Y. Liu, and C. Wang, "Numerical investigation of free oblique detonation wave induced by non-intrusive energy deposition," *AIP Adv.* **11**, 125119 (2021).